In-vivo fluorescence molecular tomography based on optimal small animal surface reconstruction

Daifa Wang (汪待发), Xin Liu (刘 欣), Yanping Chen (陈延平), and Jing Bai (白 净)*

Department of Biomedical Engineering, School of Medicine, Tsinghua University, Beijing 100084, China

**E-mail: deabj@tsinghua.edu.cn*

Received February 26, 2009

Accurate small animal surface reconstruction is important for full angle non-contact fluorescence molecular tomography (FMT) systems. In this letter, an optimal surface reconstruction method for FMT is proposed. The proposed method uses a line search method to minimize the mismatch between the reconstructed three-dimensional (3D) surface and the projected object silhouette at different angles. The results show that the mean mismatches of the 3D surfaces generated on three live anesthetized mice are all less than two charge coupled device (CCD) pixels (0.154 mm). With the accurately reconstructed 3D surface, *in-vivo* FMT is also performed.

OCIS codes: 170.6280, 170.6960, 170.3010.

doi: 10.3788/COL20100801.0082.

Fluorescence molecular tomography (FMT) is an emerging diagnosis tool for small animal research and drug discovery. By tagging regions of interest with target specific fluorescent probes, FMT may resolve three-dimensional (3D) locations and geometries of target regions, such as tumors. With the development of fluorescent probe technologies, this new technology has been widely used for gene function, proteins, enzymes, metastasis, drug discovery, and cancer detection *in-vivo*[1].

In the past years, FMT systems have evolved from the early fiber-based systems[2] to the non-contact slab-shaped system using charge coupled device (CCD)[3]. However, the fixed geometries of the above systems require matching fluids, which is inconvenient for experiments. At the same time, only limited projection angles were used in slab-shaped based systems[3]. Non-contact FMT system with full-angle projections overcomes the limited projection angles of the slab geometry. Therefore, it results in more accurate localization and quantification information of the fluorescence target[4]. Additionally, it avoids using the matching fluid and simplifies the experimental setup. For imaging systems with fixed geometry, a lot of reconstruction methods have been proposed, including the adaptive mesh base method[5,6], Newton type method[7], maximum likelihood method[8], diffuse optical tomography guided method[9], and methods for time-domain FMT[10−12]. However, when applying these reconstruction methods in *in-vivo* experiments on non-contact full-angle FMT systems, accurate mouse surface should firstly be obtained. With this surface information, the light transportation in the mouse can be predicted using the diffusion equation (DE)[2−10]. In Ref. [13], the mouse surface was obtained by using a photogrammetric 3D camera. Structured light was also used for obtaining the mouse surface in Xenogen IVIS Imaging System 200 Series[14] and the hyperspectral imaging system[15]. In full-angle non-contact imaging systems[4,16], the mouse surface can be reconstructed from white light images[17,18] or shadow images[4] captured at different angles. This technique takes full advantage of the full-angle non-contact imaging system. Thus, no extra equipment such as a photogrammetric 3D camera[13] is needed.

Radon transform with Sheep Logan filter[18] or constant filter[4] has been used for reconstructing the mouse surface. Reconstructing a two-dimensional (2D) contour using Radon transform from projection lines is to find one circumscribing polygon of the real 2D geometry. This essence determines the theoretical optimal threshold parameter for extracting the 2D contour from the back projected 2D image. However, in practical *in-vivo* experiments, the optimal parameter will be different from the theoretical one as the result of mouse breath movements and mechanical errors. A line search method is introduced in this letter to obtain an optimal parameter, which minimizes the mismatch between the reconstructed 2D contour and the projection line. Therefore, the obtained surface will be more accurate compared with that obtained with other Radon transform based surface reconstruction methods[4,18]. The optimal surface obtained will lead to better mathematical modeling of light propagation in live mice.

The full-angle non-contact imaging system[16] used in this letter is shown in Fig. 1. The imaged object was positioned on a stage which could rotate and rise. Light from a 250-W halogen lamp (7-star, Beijing) traveled through a 715-nm long-pass filter (Andover Corporation, Salem, NH) and a 775± 23-nm band-pass filter (Semrock, Rochester, NY) to provide the excitation light. The excitation light was then coupled into a 4-mm inner diameter optical fiber. The excitation light from the optical fiber was focused on the mouse back surface with a diameter less than 2 mm and a power of 13 mW. The focus point was maintained over a 9-mm depth of field, which was appropriate for irregular mouse shape. Photons which propagate out of the mouse front surface were acquired by a 512 × 512 element EMCCD array (Andor, Belfast, Northern Ireland, UK) which was

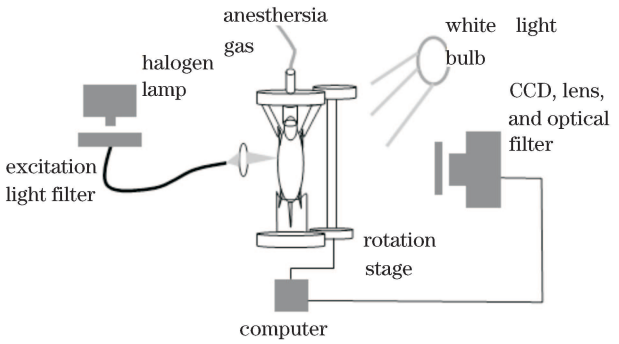

Fig. 1. Experimental setup.

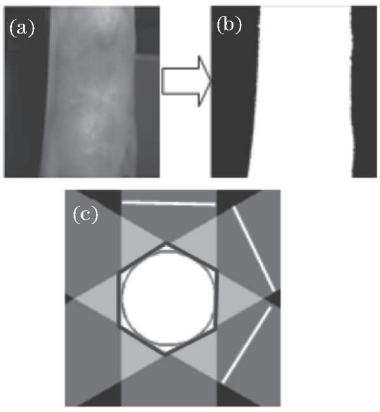

Fig. 2. Illustration of Radon transform based surface reconstruction methods. (a) The captured white light image at one projection angle; (b) the detected silhouette (binary image) from the white light image; (c) the essence of Radon transform based surface reconstruction methods.

cooled to $-70\,^{\circ}\mathrm{C}$ and coupled with a Nikkor 60-mm $f/2.8D$ lens (Nikon, Melville, NY). When the fluorescence images were recorded, a 840 ± 6-nm band-pass filter (Semrock, Rochester, NY) was placed in front of the lens. When the excitation light images were recorded, a neutral density filter (Daheng, Beijing) was placed in front of the lens to allow 6% excitation light transmission and prevent possible highlight damage to the CCD. When the white light images were recorded for surface reconstruction, the white light bulb was switched on to provide front light illumination, while the excitation light was switched off.

Before surface reconstruction, the object silhouette is detected from the captured white light image using vertical sobel gradient operator, as shown in Figs. 2(a) and (b). With the accurately detected silhouette at different angles, the 3D surface is obtained by reconstructing the 2D contour at each height slice. At each height slice, the 2D contour is obtained by back projecting all the projection lines at different angles, equivalent to the Radon transform method with a constant filter. As shown in Fig. 2(c), the circle represents the real 2D geometry. The three white lines represent the projection lines at three different angles. The back projected 2D image is generated by back projecting the projection lines. The region inside the polygon contains unity pixels. The unity pixels are the pixels which have the maximum gray values and appear in the back projected band of each projection line. Then, the polygon is the reconstructed 2D contour from the projection lines. From Fig. 2(c), we can see that reconstructing the 2D contour from the projection lines is to find one circumscribing polygon of the real 2D geometry. As the number of projection angles increases, the circumscribing polygon will approximate the real 2D geometry more accurately. Theoretically, once back projected image is obtained, the most accurate 2D geometry can be extracted by finding pixels (unity pixels) which appeared in all silhouettes. Considering that the intensity of unity pixels is 1 unit, then finding unity pixels means finding pixels with intensity value above or equal to the threshold of 1. However, in *in-vivo* experiments, the theoretically determined threshold does not produce the most accurate 2D contour due to the mouse breath movements and mechanical errors of imaging systems. For example, good results were consistently generated with threshold set to 0.8[4].

It should be noted that the mouse breath movements in different regions are different. For example, the mouse breath movements in the chest region are larger than those in the abdomen region. At the same time, the mechanical errors of different FMT systems will be different. Herein, an automatic and optimal threshold at each slice j is determined by

$$f(\mathrm{th}_j) = \min\{\sum_{\theta_i}[\left|L(j,\theta_i)_{\mathrm{left}} - \vec{L}_{\mathrm{th}}(j,\theta_i)_{\mathrm{left}}\right| + \left|L(j,\theta_i)_{\mathrm{right}} - \vec{L}_{\mathrm{th}}(j,\theta_i)_{\mathrm{right}}\right|]\}, \quad (1)$$

where $L(j,\theta_i)$ is the collected projection line at angle θ_i, and $\vec{L}_{\mathrm{th}}(j,\theta_i)$ is the calculated projection line at angle θ_i of the reconstructed 2D geometry with threshold set to "th". Subscripts "left" and "right" represent the left and right positions of the projection lines. Equation (1) finds the optimal threshold th_j by minimizing the mismatch between the reconstructed 2D geometry and detected silhouette at different angles. Because Eq. (1) is a unimodal function, one-dimensional line searching method can be used to find the optimal threshold. In this letter, the golden section method is used to search the optimal threshold during the region from 0.7 to 1.0. It should be noted that Eq. (1) does not eliminate the mouse breath movements. Instead, it obtains a mean surface which has the minimal mismatch with the detected silhouettes at different angles.

With the reconstructed 3D surface, finite element method is used to solve the diffusion equation. The normalized born method[3] is employed to correct the mouse tissue heterogeneity influences, where the measured fluorescence signals are divided by their corresponding excitation light signals. A linear system $m = Wn$ with weight matrix W can be generated[19], where m is the measured data and n is the unknown distribution of fluorescence targets. For reconstruction, the linear system is inversed using randomized algebraic reconstruction technique (R-ART).

For small animal imaging, a mouse (Kunming mouse, 4 weeks, 26 g) was firstly shaved and anesthetized under the isoflurane-air gas mixture. After that, one transparent glass tube was implanted into the mouse

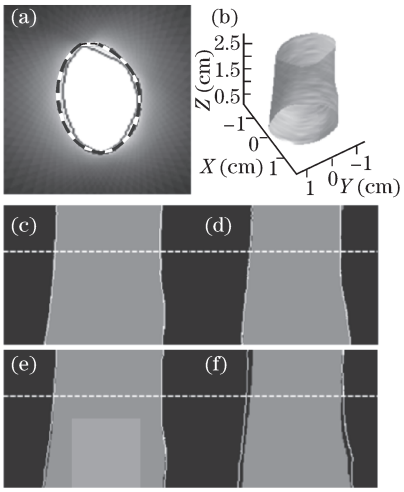

Fig. 3. Surface reconstruction results. In (a), the solid line represents the extracted 2D contour with the optimal threshold parameters, while the dashed line represents with the constant threshold 0.7[4]. (b) The extracted 3D surface with the optimal threshold is mapped to projected images at (c) 0° and (d) 55°, respectively. The extracted 3D surface with threshold 0.8 is mapped to projected images at (e) 0° and (f) 55°, respectively. White solid lines in (c)-(f) correspond to the 3D surfaces, while the gray regions indicate the detected silhouettes. Dashed lines in (c)-(f) indicate the 2D slices used in (a).

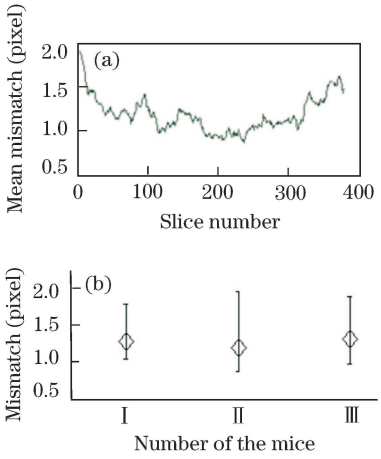

Fig. 4. The 3D surface resolution. (a) The mean mismatches of different height slices for mouse I; (b) the mean mismatches of different height slices for the three mice.

subcutaneously. The diameter of the tube was 1 mm and it was filled with 7-mm length indocyanine green (ICG) of 10-μM concentration. Then, *in-vivo* experiment was performed while keeping the mouse anesthetized under the isoflurane-air gas mixture. For white light images, 72 projections were collected every 5 degrees. For the fluorescence and excitation light images, 36 projections were collected every 10 degrees. The exposure time for excitation and emission light was 0.7 and 4.0 s, respectively. The total imaging spent 5.0 minutes approximately. White light images were also collected on another two shaved mice (Kunming mouse, 4 weeks, 25-30 g) to further investigate the reconstructed 3D surface resolution.

For mouse region between lower bottom abdomen and middle chest, the reconstructed 3D surface with optimal threshold is indicated in Fig. 3(b). In Figs. 3(c) and (d), the reconstructed 3D surface with optimal threshold is mapped to the white light images at 0 and 55 degrees, respectively. In contrast, the reconstructed 3D surface with a constant threshold 0.8[4] is also mapped to the white light images, as shown in Figs. 3(e) and (f). With the optimal threshold, the reconstructed 3D surface matches the white light images much better than that with a constant threshold 0.8. For the slices specified in Figs. 3(c)−(f), the extracted 2D contours with the optimal threshold (the solid line) and a constant threshold 0.8 (the dashed line) are shown in Fig. 3(a). For mouse I, the mean mismatches of different slices are from 1 to 2 CCD pixels, corresponding to 0.077 ∼ 0.154-mm physical dimension, as shown in Fig. 4(a). The mean mismatches of the three mice are also summarized in Fig. 4(b). The mean mismatches are all less than 2 CCD pixels.

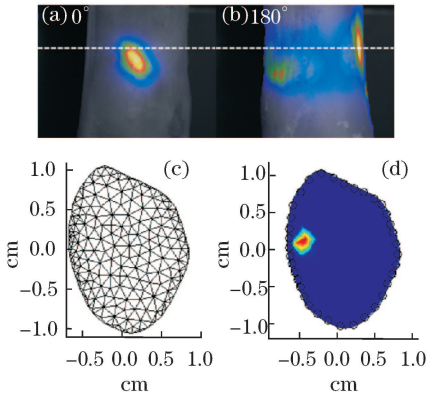

Fig. 5. *In − vivo* FMT results. (a)-(b) The collected fluorescence images overlaying on the white light images at angles of 0° and 180°; (c) the finite element mesh used; (d) reconstructed image with top 50% shown. The black circles in (d) indicate the excitation point light source. The axis unit is cm.

Figs. 5(a) and (b) show the collected fluorescence images overlaying on white light images at angles of 0° and 180°. Finite element based FMT reconstruction was performed. The optical properties of absorption coefficient $\mu_a = 0.3$ cm^{-1} and reduced scattering coefficient $\mu_s' = 10.0$ cm^{-1} were used for the reconstruction. The detector points were located on the boundary nodes in 70° field of view of the corresponding excitation point source. Data points with low signal-to-noise ratio were removed from the reconstruction. The weight matrix was generated on a finite element mesh with 372 triangle elements and 217 nodes, as shown in Fig. 5(c). 50 R-ART iterations were performed with the relaxation parameter set to 0.1. As shown in Fig. 5(d), the FMT image is well reconstructed.

In conclusion, an optimal surface reconstruction method is proposed to generate the most accurate 3D surface from the projected white light images. Results demonstrate that the proposed method generates the most accurate 3D surface with mismatch of less than 2 CCD pixels (0.154 mm) in *in-vivo* experiments. With the 3D surface, FMT tomography results are also provided. Future studies will be focused on applying the proposed method in cancer research and drug delivery.

This work was supported by the National Natural Sci-

ence Foundation of China (Nos. 30670577 and 60831003), the National Basic Research Program of China (No. 2006CB705700), the National High-Tech Research and Development Program of China (No. 2006AA020803), the China Postdoctoral Science Foundation Funded Project, and the Tsinghua-Yue-Yuen Medical Science Foundation.

References

1. V. Ntziachristos, J. Ripoll, L. Wang, and R. Weissleder, Nature Biotechnol. **23,** 313 (2005).
2. J. Chang, H. L. Graber, and R. L. Barbour, J. Opt. Soc. Am, A **14,** 288 (1997).
3. E. E. Graves, J. Ripoll, R. Weissleder, and V. Ntziachristos, Med. Phys. **30,** 901 (2003).
4. H. Meyer, A. Garofalakis, G. Zacharakis, S. Psycharakis, C. Mamalaki, D. Kioussis, E. Economou, V. Ntziachristos, and J. Ripoll, Appl. Opt. **46,** 3617 (2007).
5. J. Lee, A. Joshi, and E. M. Sevick-Muraca, Opt. Express **15,** 6955 (2007).
6. D. Wang, X. Song, and J. Bai, Opt. Express **15,** 9722 (2007).
7. R. Roy, A. Godavarty, and E. M. Sevick-Muraca, J. Biomed. Opt. **11,** 044007 (2006).
8. D. Hyde, E. Miller, D. H. Brooks, and V. Ntziachristos, IEEE Trans. Med. Imaging **26,** 893 (2007).
9. Y. Tan and H. Jiang, Appl. Opt. **47,** 2011 (2008).
10. F. Gao, L. Zhang, J. Li, and H. Zhao, Chin. Opt. Lett. **6,** 889 (2008).
11. F. Yang, Y. Ma, F. Gao, and H. Zhao, Acta Opt. Sin. (in Chinese) **28,** 1571 (2008) .
12. L. Zhang, H. He, F. Gao, and H. Zhao, Acta Opt. Sin. (in Chinese) **28,** 1262 (2008) .
13. R. B. Schulz, J. Ripoll, and V. Ntziachristos, IEEE Trans. Med. Imaging **23,** 492 (2004).
14. B. W. Rice, H. Xu, and C. Kuo, The U.S. Patent Application 20060268153 (Nov 30, 2006).
15. G. Zavattini, S. Vecchi, G. Mitchell, U. Weisser, R. Leahy, B. Pichler, D. Smith, and S. Cherry, Phys. Med. Biol. **51,** 2029 (2006).
16. G. Hu, J. Yao, and J. Bai, Prog. Nat. Sci. **18,** 707 (2008).
17. T. Lasser, A. Soubret, J. Ripoll, and V. Ntziachristos, IEEE Trans. Med. Imaging **27,** 188 (2008).
18. J. Yao, G. Hu, and J. Bai, Chin. J. Biomed. Eng. (in Chinese) **27,** 360 (2008).
19. X. Song, D. Wang, N. Chen, H. Wang, and J. Bai, Opt. Express **15,** 18300 (2007).